Forecasting when cells die during antibiotic exposure using stochastic gene expression

Nicholas A. Rossi[1,2], Imane El Meouche[2,3], Mary J. Dunlop[1,2,3,*]

[1] Molecular Biology, Cell Biology & Biochemistry Program, Boston University, Boston, Massachusetts, USA
[2] Biological Design Center, Boston University, Boston, Massachusetts, USA
[3] Department of Biomedical Engineering, Boston University, Boston, Massachusetts, USA
* Corresponding author: mjdunlop@bu.edu

Abstract
Antibiotic killing does not occur at a single, precise time for all cells within a population. Variability in time to death can be caused by stochastic expression of genes, resulting in differences in endogenous stress-resistance levels between individual cells in a population. This variability can be part of a bet-hedging strategy where cells leverage noise to ensure a subset of the population can tolerate the drug, while decreasing the overall cost of expressing resistance genes. We asked whether single-cell differences in gene expression prior to antibiotic addition were related to cell survival times after antibiotic exposure for a range of genes of diverse function. We quantified the time to death of single cells under antibiotic exposure in combination with expression of reporters. For some reporters, the time to cell death had a strong relationship with the initial expression level of the genes. Reporters that could forecast cell fate included stress response genes, but also genes involved in a variety of other cellular processes like metabolism. Our results highlight the single-cell level non-uniformity of antibiotic killing and also provide examples of key genes where cell-to-cell variation in expression prior to antibiotic exposure is strongly linked to extended durations of antibiotic survival.

Introduction
Bacteria are killed by antibiotics, but their effect is not instantaneous nor uniform. Rather, antibiotic exposure results in a distribution of killing times, with some bacteria succumbing to antibiotic exposure quickly while others remain viable. In population-level experiments this effect is visible in time-kill assays, which for *Escherichia coli* typically demonstrate rapid killing within a window of 1-3 hours following antibiotic exposure (1). However, survival of even a small number of cells can be critical in clinical settings, resulting in recalcitrant and chronic infections. A well-studied example of this is bacterial persistence, where a subset of the population exists in a temporarily dormant state that renders those bacteria tolerant to antibiotics (2). Time-kill experiments in bulk population studies result in a biphasic killing curve, with a first phase where the majority of the cells are killed rapidly, followed by a second phase where death of the remaining "persister" cells is much more gradual (3). Single-cell studies have shown these bacterial persisters can survive and regenerate populations (4,5), leading to recalcitrant infections (6). Besides the discrete persister cells, populations of bacteria can also exhibit a continuum of resistance levels. In this case, the probability of survival under antibiotic exposure changes as a function of the expression of their stress response genes (7). In addition to their clinical impact in chronic infections, cell-to-cell differences in antibiotic susceptibility can play a critical role in the evolution of drug resistance (8-10). Temporal differences in survival times are

important, as recent studies have shown that drug resistance can evolve rapidly under ideal, selective conditions (10,11).

Variability in gene expression arising from stochasticity in the order and timing of biochemical reactions is omnipresent, and populations of cells can leverage this variability (often called 'noise') to introduce phenotypic diversity despite their shared genetics (12). For example, bacteria can exhibit heterogeneity in expression of stress response genes, allowing some individuals in the population to express these genes more highly, leading to their adaptation and survival under stress (7,9,13). Examples of stress response machinery driven by noise include sporulation and competence pathways in *B. subtilis* (14-16) and lysis and lysogeny in λ phage (17). In addition, we have shown that expression of the multiple antibiotic activator MarA in *E. coli* is heterogeneous, which generates diverse resistance phenotypes within a population (7). Beyond stress response, fluctuations in gene expression can inform the future outcomes of a variety of cellular states. These include examples from development, where variability in the Notch ligand Delta can effectively forecast *Drosophilia* neuroblast differentiation (18). Additionally, knowledge of the number of lactose permease molecules in a cell can predict if individual *E. coli* induce *lac* operon genes (19). Moreover, combining information from multiple genes may increase the capacity to forecast future cell fate, as was shown in a yeast metabolic pathway (20).

Here, we measure single cell killing as a function of time under antibiotic exposure. By simultaneously measuring gene expression within single cells and cell survival, we identified genes whose instantaneous expression prior to antibiotic introduction correlates well with the ability to extend survival times under antibiotic exposure. To do this, we computed the mutual information between gene expression levels and the life expectancy of the cells expressing them. We found examples where gene expression can determine when the cell is likely to die, not simply if the cell is going to die. These results demonstrate the critical information contained within the stochastic expression of certain genes in their capacity to forecast cell fate. We analyze a variety of factors, including cell size and mean expression levels, and reveal that expression of certain genes can effectively forecast cell fate, while many other features are at best weakly predictive at informing whether the cell will live or die in the presence of antibiotics.

Results

In order to quantify the relationship between stochastic gene expression and the time to cell death under antibiotic exposure, we grew cells with a plasmid containing the promoter for a gene of interest controlling expression of cyan fluorescent protein (*cfp*). At t = 0 we transferred cells with the reporter to agarose pads containing a lethal dose of carbenicillin and then monitored cell killing over time (Methods). We selected carbenicillin because of its clinical relevance (21), and its bactericidal activity, which makes it straightforward to pinpoint the exact time of cell death (22). At t = 0 we observed heterogeneity in gene expression, as quantified by CFP fluorescence levels (Fig. 1A). We then recorded the percentage of dead cells in the population at each time point using propidium iodide. Propidium iodide enters the cells and stains DNA if the membrane is depolarized (23).

As an example, we observed a strong relationship between gene expression levels and cell killing for the *gadX* promoter. GadX is a positively auto-regulated transcription factor that controls the

expression of pH-inducible genes (24,25). Despite the fact that all imaged cells were isogenic clones, we observed heterogeneity in P_{gadX}-*cfp* expression and also in antibiotic lethality over time. The time-dependent killing curve was consistent across replicates, with cells with higher expression of P_{gadX}-*cfp* at t = 0 surviving for longer than those with low expression (Fig. 1B).

To quantify this, we sorted the cells according to their fluorescence at t = 0 from low to high expression, then binned them so that each bin contained 10% of the cells. We tracked lysis of single cells over time, to quantify the difference in time to death as a function of the initial fluorescence of the P_{gadX}-*cfp* reporter (Fig. 1C). We found that the brightest 10% of cells, corresponding to those with the highest expression of P_{gadX} prior to antibiotic exposure, survived for longer times under antibiotics than cells with lower expression (Movie S1).

Next, we extended this analysis to include additional genes, constructing reporters for a total of 15 promoters. Our analysis included genes that covered the major branches of the gene ontology classification system for *E. coli* (26) (Fig. S1). They include reporters for genes involved in metabolism, cell processes, cell structure, transport, information transfer, and regulation. We repeated the antibiotic exposure experiments for each reporter and compared time of death for single cells to the initial fluorescence level of that cell. Each reporter had a unique distribution of initial fluorescence values, and ranking and dividing cells into ten equal groups gave us an unbiased way of ranking levels of gene expression given diverse means and distributions of fluorescence (Fig. S2).

We quantified the percentage of the initial population that survived for each decile (10%) of initial fluorescence over time for all 15 promoters (Fig. 2A). Qualitatively, we observed that certain promoters have a clear relationship between the time to cell death and the fluorescence at t = 0 (P_{purA}, P_{inaA}, P_{rob}, P_{gadX}), while others die at a uniform time regardless of initial fluorescence (e.g. P_{fis}). These features are visible in the heatmaps showing the percentage of dead cells over time as a function of the initial fluorescence. Interestingly, not all reporters with predictive power about the time to cell death have the same characteristic shape to their heatmaps. For instance, some reporters show a negative relationship between cell death and fluorescence (P_{inaA}, P_{rob}, P_{gadX}) while others show a positive relationship (P_{purA}). Also, in some cases there is a distinct expression level that defines a cutoff for extended survival times (top 10% of cells for P_{gadX}, bottom 30% of cells for P_{purA}). In other cases, there is a continuous relationship between fluorescence and survival (P_{rob}). The differences in the shape of these heatmaps may reflect the biological mechanism by which these genes offer resistance.

To quantify the predictive power of each reporter in determining cell killing, we measured how the initial fluorescence decreases uncertainty about the future cell state. Because of the differences in the heatmaps, we sought to use a metric that was agnostic to the exact shape of the killing over time as a function of gene expression. To do this, we computed the mutual information between reporter florescence at t = 0 and the cellular state at each subsequent time point (Methods). To provide intuition into the results, we visualized several characteristic heatmaps (Fig. S3). If all cells are alive (as at t = 0) or if all cells are dead (as is the case after long periods of antibiotic exposure), the information is zero. If cells die linearly in precise proportion to their initial fluorescence, the corresponding information is a parabolic arc over time, where information peaks at the theoretical maximum of 1.0 bit when half the cells are dead

(Fig. S3A). Variations on this pattern decrease the information (Fig. S3B,C). Finally, if cell death is not related to initial fluorescence, then the information is always zero (Fig. S3D).

Computing the information over time allowed us to compare the predictive power of each of the 15 reporters (Fig. 2B). We found that the peak mutual information between initial fluorescence and cellular death varies among promoters. The peak information occurs at the point in the experiment where the initial fluorescence is most informative about the cellular state at that time. Considering the top four promoters when ranked by peak information (Fig. 2C) (P_{purA}, P_{inaA}, P_{rob}, P_{gadX}), we found that each peak occurs at a different time point, indicating that temporal ordering of these genes may be significant in determining cell killing. For each reporter, we also calculated the difference between cell killing times by measuring the difference in time to 50% cell killing between the decile where cells were killed fastest and that where they survived the longest (Fig. 2D). Cells containing P_{purA} and P_{inaA} reporters exhibited the greatest diversity in killing times.

We next asked if the predictive power of a particular promoter was a result of the statistics of that promoter, not its cellular function. To do this, we calculated the correlation between the peak information and its strength (mean expression) and noise (coefficient of variation) for all reporters (Fig. S4). We found no correlation between mean expression and peak information (Fig. S4A) nor any significant correlation between the coefficient of variation and peak information (Fig. S4B). These results show that the naive statistics of a promoter are not the reason why it is or is not predictive for cell fate.

We also computed the information between cell fate and cell size at t = 0, a measurement independent of the fluorescence. Cell size is variable at the initial time point because cells are at different stages in the division process. We found that initial cell size has modest predictive power about survival, and the heatmap shows slightly extended survival times for smaller cells in the presence of carbenicillin (Fig. S5). This finding on the relationship between cell size and killing time is consistent with previous research showing that the longer it has been since division, the more likely a cell is to lyse in the presence of carbenicillin (27). However, the modesty of its predictive capacity is a testament to the relative phenotypic importance of stochastic gene expression by comparison. Although this effect is present, expression of reporters like P_{purA} are far more predictive of survival than cell size.

Our initial experiments used carbenicillin, however we next asked whether results on information between gene expression and cell killing were specific to this particular stressor or extended to other antibiotics. We repeated our experiments using a subset of reporters with ciprofloxacin. Ciprofloxacin is a clinically relevant antibiotic that inhibits DNA gyrase (28). Unlike carbenicillin, it exhibits both bactericidal and bacteriostatic affects (29). Comparing the peak mutual information between six of the promoters with the two antibiotics, we found distinct differences between their predictive power for carbenicillin and ciprofloxacin (Fig. 3A). First, P_{gadX} has a peak mutual information of ~0.3 bits under ciprofloxacin treatment. This is considerably more than the information P_{gadX} provides under carbenicillin. Contrary to this, P_{purA}, P_{inaA}, and P_{rob} all offer more predictive power under carbenicillin stress than ciprofloxacin. $P_{\sigma 70}$ and P_{hdeA} offer comparable predictive power between the two antibiotics, with the constitutive promoter $P_{\sigma 70}$ providing negligible capacity to forecast cell fate in either case. The heatmaps

from both antibiotics also show qualitative differences in how reporters predict cell fate. For instance, while cells with comparatively high P_{gadX} fluorescence survive well in both carbenicillin and ciprofloxacin, it is only the top decile of cells in carbenicillin that have a comparative advantage, while the upper half do in ciprofloxacin. The opposite proves true for P_{hdeA} where only the lowest decile of cells have an advantage in ciprofloxacin, but a there is a continuous advantage as a function of lower fluorescence in carbenicillin. Together, these results show that although gene expression may correlate well with cell death, the time to death and single-cell level killing effects can vary considerably with the type of stress.

Discussion

We have demonstrated that differences in gene expression associated with noisy promoter activity have the potential to forecast information about the future fate of a cell. This approach allowed us to quantify how phenotypically meaningful the stochastic expression of a particular promoter is for survival in the presence of antibiotics. The promoters we selected for our reporters occupy a variety of roles. Of those we tested, reporters for metabolism, cell processes, and information transfer had the most predictive power (Fig. S6), however not every promoter within those classes is predictive. Surprisingly, some genes known to be involved in antibiotic resistance were not detected to have a strong relationship to when the cells died. For instance, the reporter for the *acrAB* multi-drug efflux pump had a low peak information value, despite the pump's ability to export both carbenicillin and ciprofloxacin (30). This could be because promoter activity is not necessarily representative of actual proteins within the cell, where direct measurements of protein levels would provide better information (31). Alternatively, the advantages of additional *acrAB* at the levels provided due to endogenous variability in promoter activity may simply be too subtle to produce a detectable phenotypic difference.

Interestingly, we observed some variation in the exact killing curves between the strains with the reporters (Fig. S7A). Some strains were killed more rapidly than others, and this effect was reproducible across replicates. While the time to reach 50% dead cells does vary among strains bearing the reporter plasmids, this time does not correlate with their peak information (Fig. S7B). The exact source of the variation in killing curves is unclear, but it may be that the promoter copies on the reporter plasmids operate as competitive binding sites for transcription factors and other cellular machinery necessary for resistance (32).

An additional question raised by this work is whether the information offered by the various reporters could be used together to further improve predictions about time to cell death. To tackle this problem, the notion of multivariate information could be applied to include multiple genetic reporters (33). If multiple reporters contain non-redundant information about cell fate, it may be possible to predict the outcome of a cell based on sufficient initial data, even prior to antibiotic exposure.

By showing how life expectancy varies as a function of initial fluorescence, we demonstrate an important relationship between gene expression and time to cell death across genes of varying function. Differences in the time to death are important because they may point to underlying mechanisms by which a particular gene grants resistance and could expose potential gateways in the evolution of drug resistance. Expanding this research to include additional reporters and

antibiotics has the potential to provide a global overview of how stochasticity in gene expression propagates to variability in survival times.

Methods

Plasmids and Strains

All reporter plasmids have a low-copy SC101 origin of replication with a kanamycin resistance cassette and a promoter transcriptionally controlling cyan fluorescent protein (*cfp*). We isolated each promoter region based on annotations in the EcoCyc database (34). The selected sequences include all known regulatory binding sites within the database. In the absence of any binding annotations, we selected a 200 bp fragment ending with the transcriptional start site. For primers, see Supplementary Information.

All plasmids were transformed into *E. coli* strain MG1655.

Time-lapse Microscopy

Overnight cultures were grown from single colonies in LB medium with 30 µg/ml kanamycin for plasmid maintenance. From these cultures, a 1:100 dilution was used to inoculate fresh LB with kanamycin. Cultures were incubated for 4 hrs at 37 °C with shaking. Cells were then diluted 3:10 in M9 minimal medium containing 0.2% glycerol, 0.01% casamino acids, 0.15 µg/ml biotin, and 1.5 µM thiamine (which we denote MGC medium). Cells were then placed on 1.5% MGC low melting temperature agarose pads contain either 50 µg/ml carbenicillin or 2 µg/ml ciprofloxacin along with 10 µg/ml propidium iodide. Cells were imaged at 100× using a Nikon Instruments Ti-E microscope. The temperature of the microscope chamber was held at 32 °C for the duration of the movies. Images were taken every 5 minutes for 5 hours for at least 5 pad positions per strain, with each image containing ~100 cells.

We tracked cell death by a combination of custom MATLAB scripts and manually scanning through the movies to locate the time of death. Our MATLAB scripts adapted the SuperSegger software for the initial segmentation (35). We used propidium iodide fluorescence as well as other visual markers (loss of contrast in phase images, compromises to the cell wall) to ascertain the moment of cell death.

Computing Mutual Information

We compute the mutual information between cellular state (alive or dead) at time t (x_t) and the initial fluorescence of that cell for a given promoter (y).

$$I(x_t, y) = H(x_t) - H(x_t|y)$$

We compute the entropy of x_t from the binary entropy formula. $p(x_t)$ is computed as a fraction of cells dead at time t, across all initial fluorescence values for that time point.

$$H(x_t) = -p(x_t)\log_2 p(x_t) - (1 - p(x_t))\log_2(1 - p(x_t))$$

Finally, the conditional entropy is computed for a given initial fluorescence level (y_i). Where i is one of the ten deciles of initial fluorescence (Fig. S2). We then average the conditional entropy across all fluorescence bins to calculate the average conditional entropy over time. We optimized

the number of bins given the number of individual cells analyzed for each strain (~500 cells) (36).

$$H(x_t|y) = \frac{1}{n}\sum_{i=1}^{n} -p(x_t|y_i)\log_2 p(x_t|y_i) - (1-p(x_t|y_i))\log_2(1-p(x_t|y_i))$$

Gene Ontology

To map our data to the functions of each gene, we looked up the role of each gene from the multifunctional classification scheme (26,34). We pooled the categories of information transfer and regulation, as they were entirely overlapping for the promoters we selected.

Acknowledgements

We thank Pankaj Mehta for helpful discussions. This work was supported by the National Institutes of Health grant R01AI102922 and National Science Foundation grant 1347635.

References

1. Tuomanen E, Cozens R, Tosch W, Zak O, Tomasz A. The rate of killing of Escherichia coli byβ-lactam antibiotics is strictly proportional to the rate of bacterial growth. Microbiology. 1986 May 1;132(5):1297-304.

2. Balaban NQ, Merrin J, Chait R, Kowalik L, Leibler S. Bacterial Persistence as a Phenotypic Switch. Science. American Association for the Advancement of Science; 2004 Sep 10;305(5690):1622–5.

3. Lewis K. Persister cells. Annual review of microbiology. 2010 Oct 13;64:357-72.

4. Maisonneuve E, Gerdes K. Molecular Mechanisms Underlying Bacterial Persisters. Cell. Cell Press; 2014 Apr 24;157(3):539–48.

5. Pu Y, Zhao Z, Li Y, Zou J, Ma Q, Zhao Y, Ke Y, Zhu Y, Chen H, Baker MA, Ge H. Enhanced efflux activity facilitates drug tolerance in dormant bacterial cells. Molecular cell. 2016 Apr 21;62(2):284-94.

6. Fisher RA, Gollan B, Helaine S. Persistent bacterial infections and persister cells. Nature Reviews Microbiology 2006 4:7. Nature Publishing Group; 2017 Aug 1;15(8):453–64.

7. Meouche El I, Siu Y, Dunlop MJ. Stochastic expression of a multiple antibiotic resistance activator confers transient resistance in single cells. Sci Rep. 2016;6:19538.

8. Levin BR, Rozen DE. Non-inherited antibiotic resistance. Nature Reviews Microbiology 2006 4:7. Nature Publishing Group; 2006 Jul;4(7):556–62.

9. Meouche El I, Dunlop MJ. Heterogeneity in efflux pump expression predisposes antibiotic-resistant cells to mutation. Science. American Association for the Advancement of Science; 2018 Nov 9;362(6415):686–90.

10. Levin-Reisman I, Ronin I, Gefen O, Braniss I, Shoresh N, Balaban NQ. Antibiotic tolerance facilitates the evolution of resistance. Science. American Association for the Advancement of Science; 2017 Feb 9;355(6327):eaaj2191–830.

11. Baym M, Lieberman TD, Kelsic ED, Chait R, Gross R, Yelin I, et al. Spatiotemporal microbial evolution on antibiotic landscapes. Science. American Association for the Advancement of Science; 2016 Sep 9;353(6304):1147–51.

12. Elowitz MB, Levine AJ, Siggia ED, Swain PS. Stochastic gene expression in a single cell. Science. 2002 Aug 16;297(5584):1183–6.

13. Locke JCW, Young JW, Fontes M, Jiménez MJH, Elowitz MB. Stochastic Pulse

Regulation in Bacterial Stress Response. Science. American Association for the Advancement of Science; 2011 Oct 21;334(6054):366–9.

14. Schultz D, Wolynes PG, Ben Jacob E, Onuchic JN. Deciding fate in adverse times: Sporulation and competence in Bacillus subtilis. Proceedings of the National Academy of Sciences. National Acad Sciences; 2009 Dec 15;106(50):21027–34.

15. Kuchina A, Espinar L, Garcia-Ojalvo J, Süel GM. Reversible and Noisy Progression towards a Commitment Point Enables Adaptable and Reliable Cellular Decision-Making. Covert MW, editor. PLoS Comput Biol. Public Library of Science; 2011 Nov 10;7(11):e1002273.

16. Kuchina A, Espinar L, Çağatay T, Balbin AO, Zhang F, Alvarado A, et al. Temporal competition between differentiation programs determines cell fate choice. Molecular Systems Biology. EMBO Press; 2011 Jan 1;7(1):557–7.

17. Cao Y, Lu H-M, Liang J. Probability landscape of heritable and robust epigenetic state of lysogeny in phage lambda. Proceedings of the National Academy of Sciences. National Academy of Sciences; 2010 Oct 4;107(43):18445–50.

18. Losick R, Desplan C. Stochasticity and Cell Fate. Science. American Association for the Advancement of Science; 2008 Apr 4;320(5872):65–8.

19. Choi PJ, Cai L, Frieda K, Xie XS. A stochastic single-molecule event triggers phenotype switching of a bacterial cell. Science. 2008 Oct 17;322(5900):442-6.

20. Argüello-Miranda O, Liu Y, Wood NE, Kositangool P, Doncic A. Integration of Multiple Metabolic Signals Determines Cell Fate Prior to Commitment. Molecular Cell. Cell Press; 2018 Sep 6;71(5):733–744.e11.

21. Turck M, Silverblatt F, Clark H, Holmes K. The role of carbenicillin in treatment of infections of the urinary tract. The Journal of infectious diseases. 1970 Sep 1:S29-33.

22. Tomasz A. The mechanism of the irreversible antimicrobial effects of penicillins: how the beta-lactam antibiotics kill and lyse bacteria. Annual Reviews in Microbiology. 1979 Oct;33(1):113-37.

23. Ueckert J, Breeuwer P, Abee T, Stephens P, Caron von GN, Steeg ter PF. Flow cytometry applications in physiological study and detection of foodborne microorganisms. International Journal of Food Microbiology. Elsevier; 1995 Dec 1;28(2):317–26.

24. Tramonti A, De Canio M, De Biase D. GadX/GadW-dependent regulation of the Escherichia coli acid fitness island: transcriptional control at the gadY–gadW divergent promoters and identification of four novel 42 bp GadX/GadW-specific

binding sites. Mol Microbiol. Wiley/Blackwell (10.1111); 2008 Nov 1;70(4):965–82.

25. Tramonti A, Visca P, De Canio M, Falconi M, De Biase D. Functional Characterization and Regulation of gadX, a Gene Encoding an AraC/XylS-Like Transcriptional Activator of the Escherichia coli Glutamic Acid Decarboxylase System. J Bacteriol. American Society for Microbiology Journals; 2002 May 15;184(10):2603–13.

26. Serres MH, Riley M. MultiFun, a multifunctional classification scheme for Escherichia coli K-12 gene products. Microbial & comparative genomics. 2000;5(4):205-22.

27. Lambert G, Kussell E. Quantifying Selective Pressures Driving Bacterial Evolution Using Lineage Analysis. Phys Rev X. American Physical Society; 2015 Feb 17;5(1):011016.

28. Drlica K, Zhao X. DNA gyrase, topoisomerase IV, and the 4-quinolones. Microbiol Mol Biol Rev. American Society for Microbiology; 1997 Sep;61(3):377–92.

29. Silva F, Lourenço O, Queiroz JA, Domingues FC. Bacteriostatic versus bactericidal activity of ciprofloxacin in *Escherichia coli* assessed by flow cytometry using a novel far-red dye. The Journal of Antibiotics 2011 64:4. Nature Publishing Group; 2011 Apr 1;64(4):321–5.

30. Nikaido H. Antibiotic resistance caused by gram-negative multidrug efflux pumps. Clinical Infectious Diseases. 1998 Aug 1;27(Supplement_1):S32-41.

31. Bergmiller T, Andersson AMC, Tomasek K, Balleza E, Kiviet DJ, Hauschild R, et al. Biased partitioning of the multidrug efflux pump AcrAB-TolC underlies long-lived phenotypic heterogeneity. Science. American Association for the Advancement of Science; 2017 Apr 21;356(6335):311–5.

32. Stamatakis M, Adams RM, Balázsi G. A common repressor pool results in indeterminacy of extrinsic noise. Chaos: An Interdisciplinary Journal of Nonlinear Science. 2nd ed. American Institute of Physics; 2011 Dec 29;21(4):047523.

33. Timme N, Alford W, Flecker B, Beggs JM. Synergy, redundancy, and multivariate information measures: an experimentalist's perspective. J Comput Neurosci. Springer US; 2013 Jul 3;36(2):119–40.

34. Keseler IM, Mackie A, Santos-Zavaleta A, Billington R, Bonavides-Martínez C, Caspi R, Fulcher C, Gama-Castro S, Kothari A, Krummenacker M, Latendresse M. The EcoCyc database: reflecting new knowledge about Escherichia coli K-12. Nucleic acids research. 2016 Nov 29;45(D1):D543-50.

35. Stylianidou S, Brennan C, Nissen SB, Kuwada NJ, Wiggins PA. SuperSegger: robust image segmentation, analysis and lineage tracking of bacterial cells. Mol Microbiol. 2016 Nov;102(4):690–700.

36. Cellucci CJ, Albano AM, Rapp PE. Statistical validation of mutual information calculations: Comparison of alternative numerical algorithms. Phys Rev E. 2005 Jun 22;71(6):066208–15.

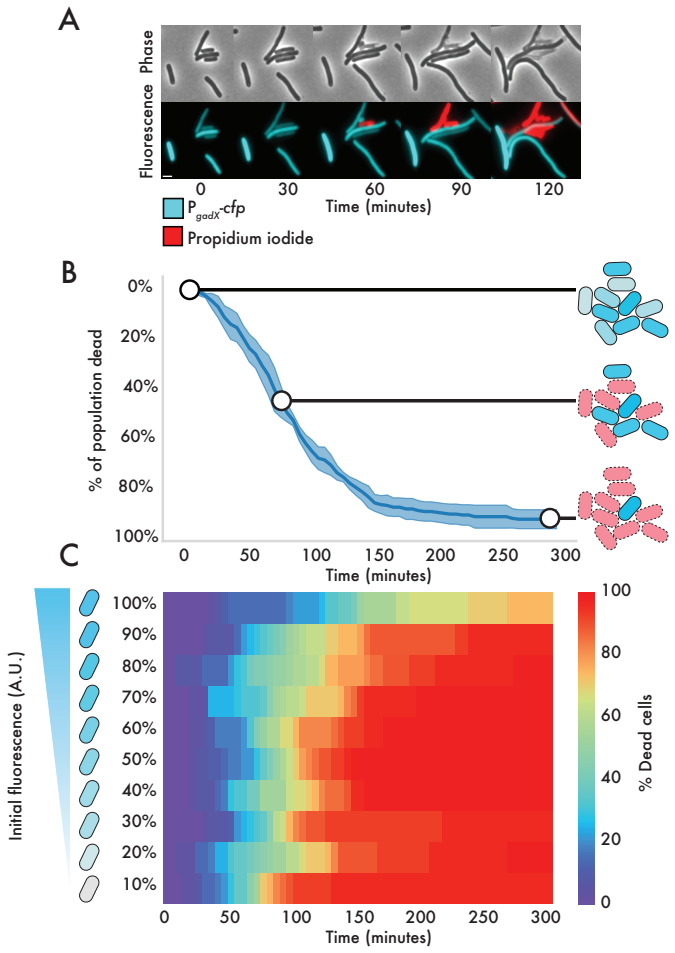

Figure 1: Differences in single-cell carbenicillin susceptibility.

(A) Snapshots of cells demonstrate variable lethality of carbenicillin. P_{gadX}-*cfp* fluorescence (cyan); propidium iodide is a cell death marker (red).

(B) Cellular populations die progressively after carbenicillin exposure. Line represents mean killing curve as a function of time. Shaded region represents standard deviation across 5 replicate microscopy positions containing ~100 cells each. Cartoon schematic demonstrates how lethality is variable among individuals within the population, but depends on initial P_{gadX}-*cfp* fluorescence.

(C) Cells die at different times as a function of their initial P_{gadX}-*cfp* fluorescence. x-axis shows the cumulative percentage of dead cells at each time point. Initial fluorescence at t = 0 is split in deciles with equal numbers of cells in each of the 10 bins along y-axis (Fig. S2).

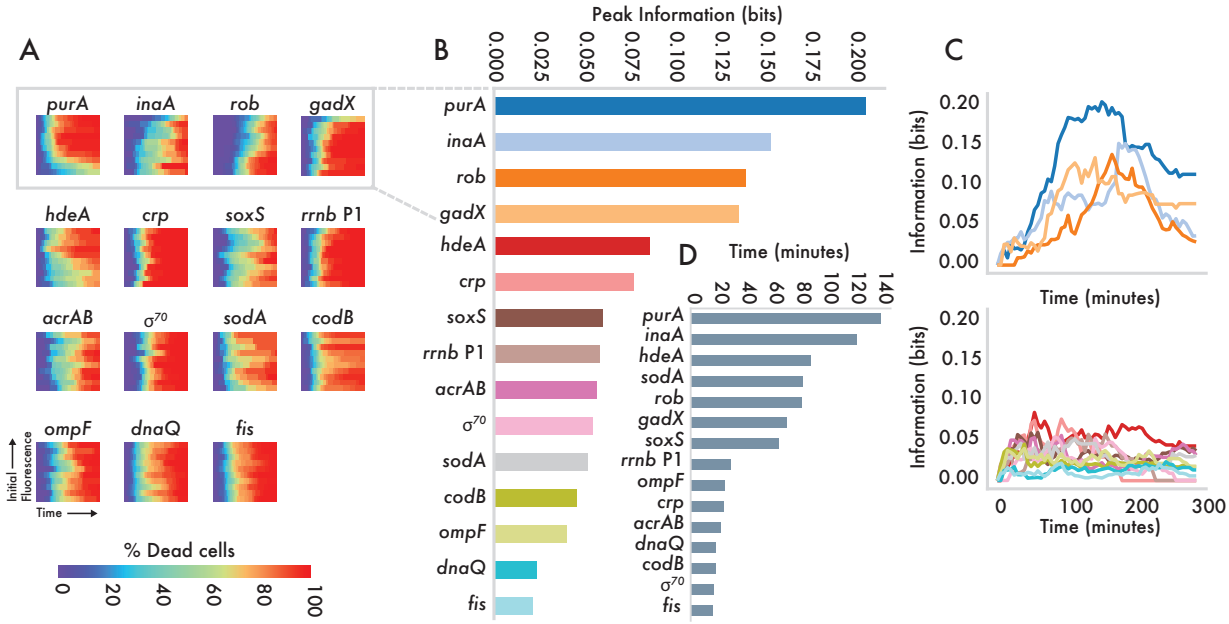

Figure 2: Different bacterial promoters have different predictive power in the presence of carbenicillin.

(A) Variable death times of cells depending on initial fluorescence. As in Fig. 1C, x-axis shows cumulative percentage of dead cells over time and y-axis represents binned deciles according to initial fluorescence at t = 0. For the bins and initial fluorescence distributions for each reporter see Fig. S2. At least 5 replicate microscopy positions with ~100 cells each were pooled before binning.

(B) Peak mutual information between initial fluorescence and cell fate for each reporter strain.

(C) Information over time for each strain. For visual clarity, the data are divided onto two plots, one of which shows the four reporters with the highest peak information and the other showing the remaining reporter data.

(A) Differences in time to reach 50% cell death between the fluorescence decile with the fastest dying cells and the decile with the slowest dying cells. Savitzky-Golay filter was used to smooth data across deciles before calculating minimum and maximum values.

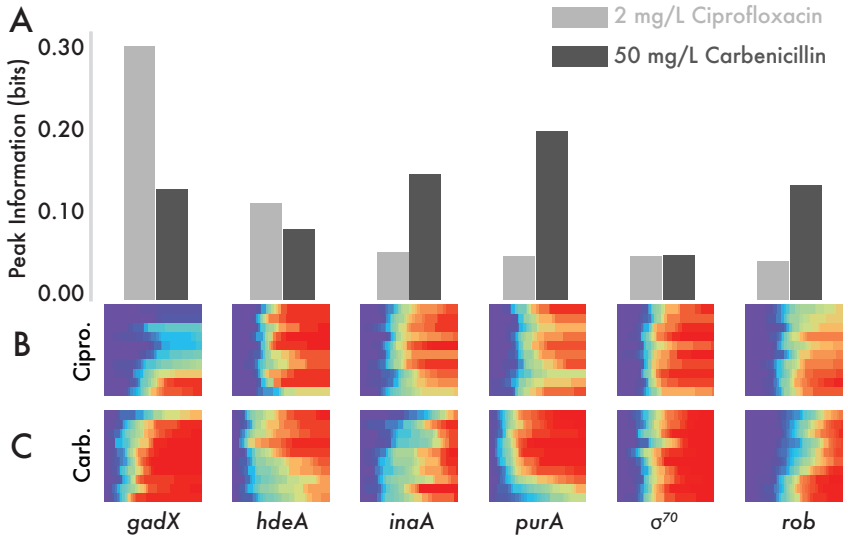

Figure 3: Promoters show different predictive power under ciprofloxacin versus carbenicillin.

(A) Peak mutual information for ciprofloxacin and carbenicillin.

(B) Variable death times for six strains under ciprofloxacin treatment. Binning on x and y-axes performed as in Fig. 1C.

(C) Variable death times under carbenicillin treatment. Data are reproduced from Fig. 2A for comparison.

Supplementary Information

Construct	Primers
P_{purA}	F: TTTATACAGTTCATCCATGCCCAGG R: CCTGGGCATGGATGAACTGTATAA
P_{inaA}	F: CAATGCTTTTCAGCGTTAACTCTG R: ACGACAATGACTATAGGTGGT
P_{rob}	F: CAAAATCTCAATACTTTTATTTCCG R: TAATTGGATAATAGCATTTTTTGC
P_{gadX}	F: GTTGACTACCTGGGTGGTC R: ACTGTTTATTAATGTAGCACGCC
P_{hdeA}	F: CCCCTGCTATCAATCTATGC R: CACTGAGGTTATAACCTGGTTTTC
P_{crp}	F: ACAGAGTACGCGTACTAACCAAATC R: GGGCTATCAACTGTACTGCAC
$P_{\sigma 70}$	F: AATAATTCTTGACATTTATGCTTCCG R: AATTGCACGTATTATACGAGC
$P_{rrnb\ P1}$	F: CTGAACAATTATTGCCCGTTTTACAG R: GAATTAAACTTCGTAATGAATTACGTGTTC
P_{acrAB}	F: GCCAGTAGATTGCACCGCG R: TCGTGCTATGGTACATACATTCACA
P_{sodA}	F: GGCAATCACGGCATTAAG R: TTGGTTCATTATAGTTAATTAAATG
P_{soxS}	F: CACGTTTATATCGCCGCTGATTG R: TGTTGGGGAGTATAATTCCTCAAG
P_{codB}	F: GATAATTTTTCCCCCACCTTTTTGC R: CCGCCGCATTCTATTCATCTG
P_{ompF}	F: CAAGTTATCTGTTTGTTAAGTCAAGCAATC R: TGCAGGCATCTTTCCATTCAAAC
P_{dnaQ}	F: GTTATGGATCCACTGGGTGATAC R: CGCTATTTTACGCTATCGCGG
P_{fis}	F: GCGAAGTGCGAGCAAGC R: AGTTAAGAAATGACCATACTGTGACTGC

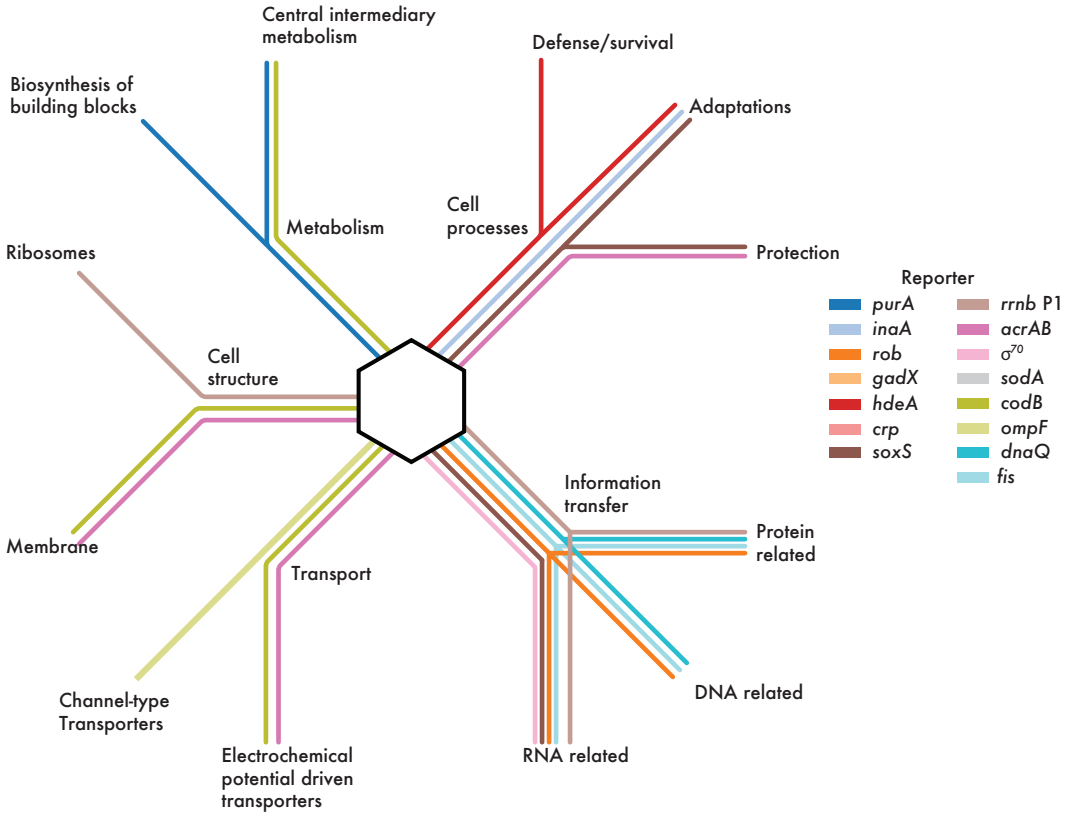

Figure S1: Genetic ontology map for the 15 promoters selected for study.
The genetic ontology of each promoter is represented as a line connecting it through to each of its functional roles in the cell (Methods).

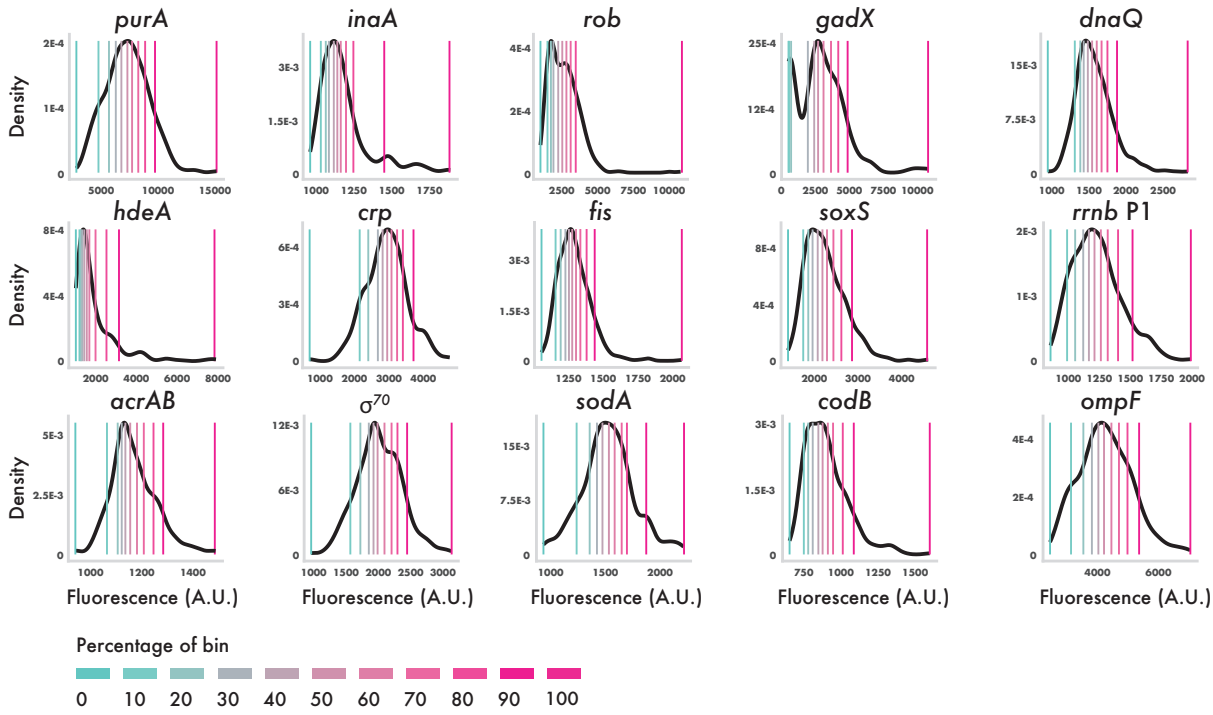

Figure S2: Distributions and decile bins for all 15 promoters tested.
Gray lines show histograms of the distributions of initial fluorescence at t = 0 for each of the 15 promoters. The colored lines show where each of the decile bins fall.

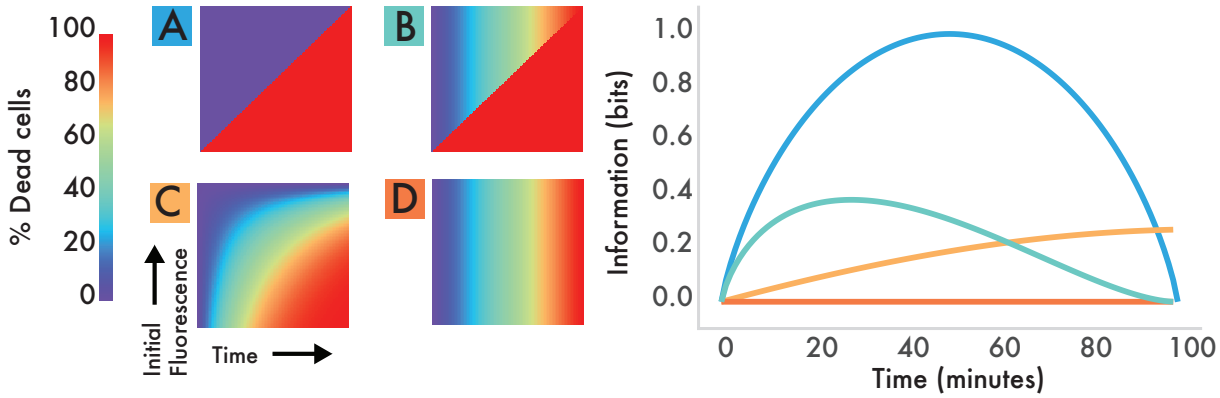

Figure S3: Schematics of heatmaps showing variable information over time.
Cartoon heatmaps of possible experimental patterns. **A** demonstrates a perfect split between alive and dead cells; the theoretical maximum information (1.0 bits) is achieved at the time of 50% cell death. **B** and **C** represent variations on this pattern. **D** demonstrates a heatmap schematic with the minimum information (0.0 bits) contained in initial fluorescence. Plots in the right panel show information over time for each of the heatmaps.

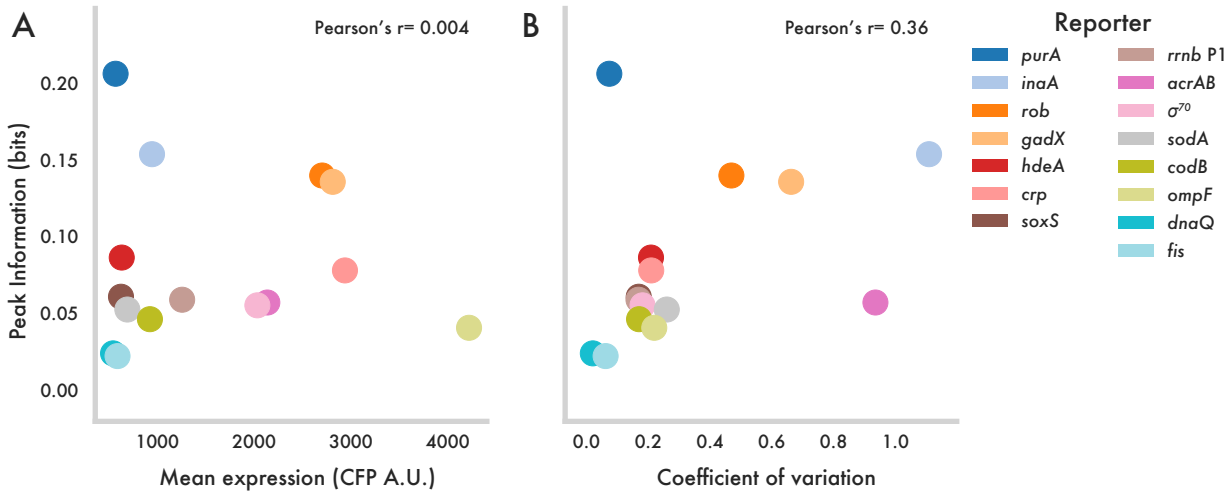

Figure S4: Relationships between reporter statistics and information.

(A) Scatter plot for all 15 strains' mean expression versus peak information from Fig. 2B. Mean expression data taken from microscopy snapshots of each strain under the same CFP exposure time to ensure comparable statistics. Pearson's r-value calculates linear correlation between the two values (1.0 = positively correlated, 0.0 = uncorrelated).

(B) Scatter plot of coefficient of variation versus peak information for each of the promoters.

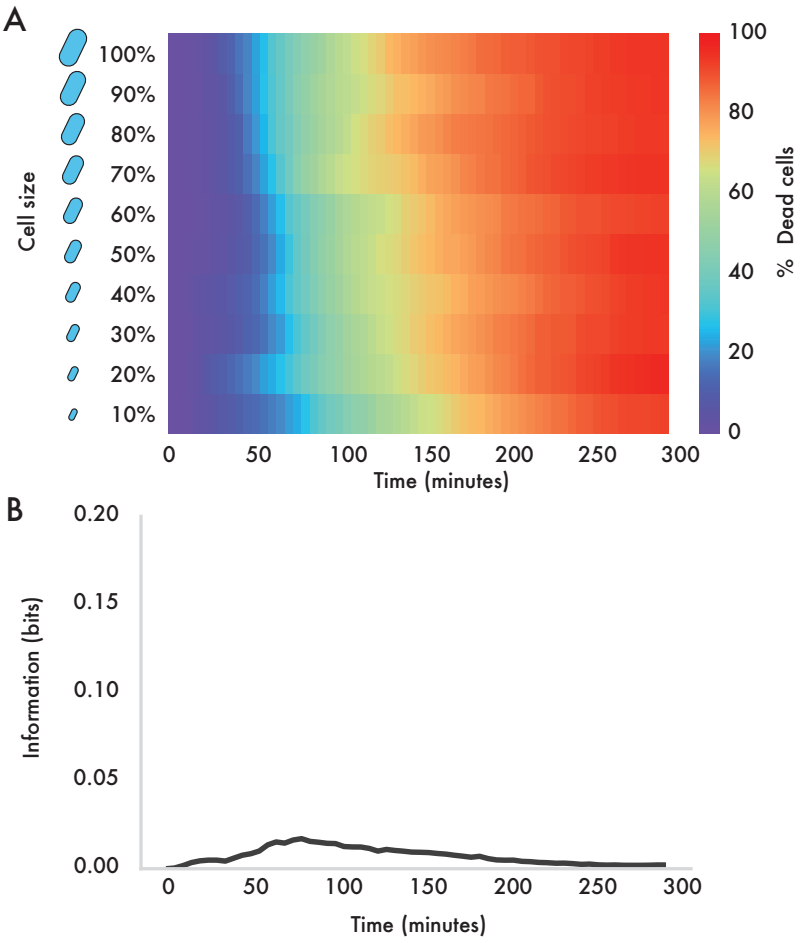

Figure S5: Cell size as a predictor of cell fate.

(A) Heatmap that mirrors Fig. 1C but uses initial cell size instead of fluorescence on the y-axis. Data are pooled from all carbenicillin reporter experiments.

(B) Information over time for cell size.

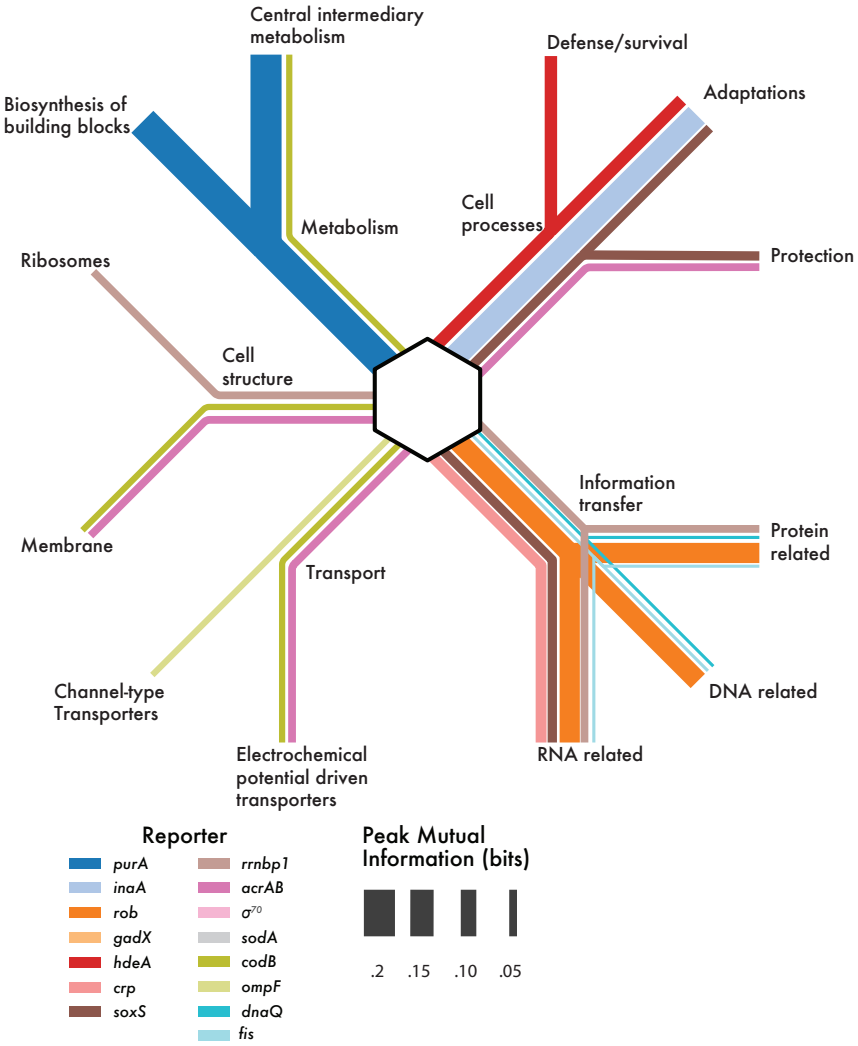

Figure S6: Peak information from carbenicillin experiments mapped onto gene ontology. The gene ontology map from Fig. S1 with the thickness of each connection dependent on the peak information from the carbenicillin data in Fig. 2B.

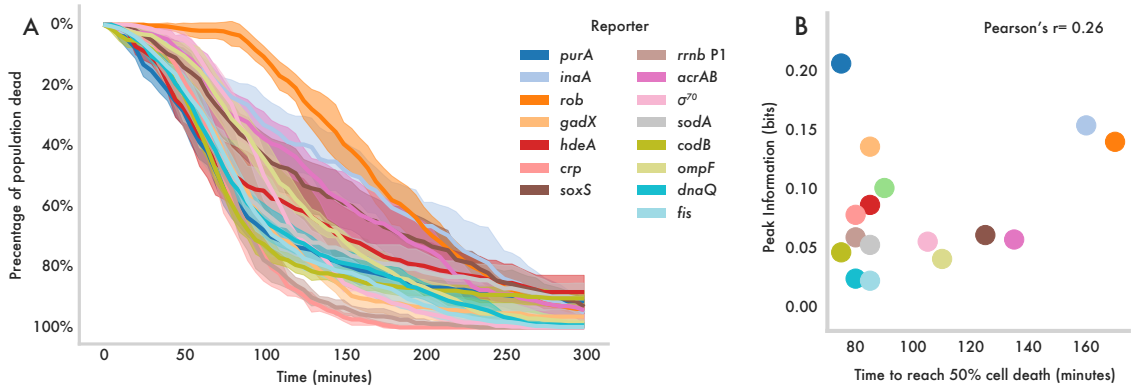

Figure S7: Killing curves for all reporter strains over time under carbenicillin.

(A) Killing curves for each strain extracted from time-lapse microscopy data. Solid lines represent the mean for at least 5 replicates while the shaded region represents the standard deviation across replicates.

(B) Scatter plot of time to reach 50% cell death versus peak mutual information. Pearson's r-value calculates linear correlation.

Movie S1: Single-cell death under carbenicillin exposure for P_{gadX}-*cfp*.

(A) Cell death over time. Red dot indicates particular point in time.

(B) Example microscopy movie of cells expressing P_{gadX}-*cfp* reporter (cyan) under carbenicillin exposure. Cell death is indicated by propidium iodide staining (red).

(C) Heatmap of cell death over time as a function of fluorescence at t = 0. White bar indicates particular point in time.

(D) Image showing fluorescence of individual cells at t = 0. As cells die they are eliminated from the image. Note that brighter cells tend to survive longer than dim cells.